ChemPubSoc Europe

DOI: 10.1002/ejic.201900727

EurJIC European Journal of Inorganic Chemistry

Full Paper

Pincer Complexes | *Very Important Paper* |

Probing the Donor Properties of Pincer Ligands Using Rhodium Carbonyl Fragments: An Experimental and Computational Case Study

Gemma L. Parker,[a] Samantha Lau,*[a] Baptiste Leforestier,[a] and Adrian B. Chaplin*[a]

Abstract: Metal carbonyls are commonly employed probes for quantifying the donor properties of monodentate ligands. With a view to extending this methodology to *mer*-tridentate "pincer" ligands, the spectroscopic properties [ν(CO), δ_{13C}, $^1J_{RhC}$] of rhodium(I) and rhodium(III) carbonyl complexes of the form [Rh(pincer)(CO)][BAr^F_4] and [Rh(pincer)Cl_2(CO)][BAr^F_4] have been critically analysed for four pyridyl-based pincer ligands, with two flanking oxazoline (NNN), phosphine (PNP), or N-heterocyclic carbene (CNC) donors. Our investigations indicate that the carbonyl bands of the rhodium(I) complexes are the most diagnostic, with frequencies discernibly decreasing in the order NNN > PNP > CNC. To gain deeper insight, a DFT-based energy decomposition analysis was performed and identified important bonding differences associated with the conformation of the pincer backbone, which clouds straightforward interpretation of the experimental IR data. A correlation between the difference in carbonyl stretching frequencies $\Delta\nu$(CO) and calculated thermodynamics of the Rh^I/Rh^{III} redox pairs was identified and could prove to be a useful mechanistic tool.

Introduction

The use of pincer ligands as scaffolds for transition metal complexes is ubiquitous in contemporary inorganic chemistry.[1–5] These rigid *mer*-tridentate ligands confer thermal stability, whilst supporting a wide range of metal-based reactivity, making them attractive ancillaries for applications in demanding organometallic chemistry and homogeneous catalysis. Pincer ligands are readily adapted, enabling the steric and electronic properties of metal derivatives to be augmented through changes to the constituent donor groups, their substituents or the backbone conformation itself.[6] The impact of such changes can, however, be difficult to gauge in a quantitative manner and frustrate the systematic optimisation of metal-based reactivity.

The use of spectroscopic reporter groups is a common approach to gauge the donor abilities of monodentate ligands, with Tolman's electronic parameter the archetypal and textbook example.[7,8] Although originally based on the carbonyl stretching frequencies of [Ni(CO)$_3$L], that are readily acquired using IR spectroscopy, this parameter is now typically ascertained using less toxic complexes of the form *cis*-[IrCl(CO)$_2$L] or *cis*-[RhCl(CO)$_2$L].[9–13] Other contemporary examples by Huynh and Bendix have exploited the palladium–carbene and platinum–carbide bonds of *trans*-[PdBr$_2$(*i*Pr-bimy)L] (*i*Pr-bimy = 1,3-diisopropylbenzimidazolin-2-ylidene) and [$(Cy_3P)_2Cl_2Ru{\equiv}C{-}PtCl_2{-}$L] as reporter groups, that can be readily interrogated using ^{13}C NMR spectroscopy (δ_{13C} and $^1J_{PtC}$).[14,15] The systematic extension of such methodologies to pincer ligands is very limited, with recent studies by Ozerov – who explored the electronic properties of a series of neutral Rh^I complexes [Rh(PND)(CO)] (D = imine or phosphine donor) – and Langer – who studied the effect of changing the central E donor group in diphenylphosphino-based PEP pincer ligands in iridium(III) hydride complexes of the form $[Ir(PEP)Cl(CO)H]^n$ (n = 0, +1, +2) – the most notable.[16,17]

To this end, we herein present our work ascertaining the capacity of rhodium(I) and rhodium(III) carbonyl fragments to probe the *net* donor properties of pincer ligands with different flanking groups: aiming to exploit convenient IR and ^{13}C NMR spectroscopic handles associated with coordination of CO to rhodium (Figure 1). As part of our research exploring the organometallic chemistry of NHC-based CNC ligands, which are becoming an increasingly prominent pincer class,[2] we have previously reported rhodium carbonyl adducts **1a**,**b** and **2a**,**b**.[18] The synthesis and characterisation of rhodium carbonyl complexes of phosphine-based *i*Pr-PNP (**3a**,**b**) and (*R*,*R*)-Ph-pybox NNN (**4a**,**b**) pincer ligands is now reported. Although this set is not extensive, it comprises widely used terminal donor combinations and is suitably diverse to make for meaningful critical analysis. DFT calculations have been used to gain molecular insight, in particular exploiting the extended transition state method for energy decomposition analysis combined with the natural orbitals for chemical valence theory (ETS-NOCV) to de-

[a] *Department of Chemistry, University of Warwick, Gibbet Hill Road, Coventry CV4 7AL, UK*
E-mail: samantha.lau@warwick.ac.uk
a.b.chaplin@warwick.ac.uk
http://go.warwick.ac.uk/abchaplin

Supporting information and ORCID(s) from the author(s) for this article are available on the WWW under https://doi.org/10.1002/ejic.201900727.

convolute contributions from σ- and π-bonding and help establish structure-property relationships.

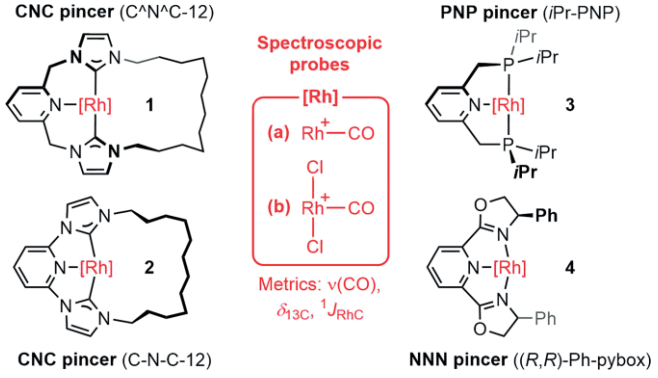

Figure 1. Pincer ligands of interest and their rhodium carbonyl derivatives. $[BAr^F_4]^-$ counter anions omitted for clarity.

Results and Discussion

1. Synthesis and Solid-State Structures of PNP and NNN Pincer Complexes

Our chosen approach for the synthesis of **3** and **4** is outlined below in Scheme 1 and centres on halide abstraction reactions of rhodium chloride complexes, using $Na[BAr^F_4]$ in the weakly coordinating C_6H_5F solvent (FB).[19] The necessary rhodium(I) chloride complexes were readily accessed by substitution of $[Rh(cyclooctene)_2Cl]_2$ with the chosen pincer ligand and subsequently oxidised to the rhodium(III) trichloride derivatives, using the easy to handle reagent $PhICl_2$,[20] which were isolated in high yield [L = *i*Pr-PNP, 84 %; (*R*,*R*)-Ph-pybox, 79 %]. The structural formulation of all four complexes was corroborated in solution by NMR spectroscopy and in the solid state using single-crystal X-ray diffraction (structures provided in the Supporting Information), with spectroscopic data of the previously reported [Rh(*i*Pr-PNP)Cl] and [Rh{(*R*,*R*)-Ph-pybox}Cl_3] in good agreement with the literature.[21,22]

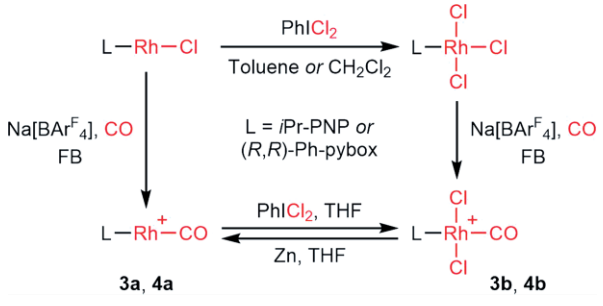

Scheme 1. Synthesis of rhodium carbonyl complexes **3** and **4**.

Halide abstraction from the rhodium(I) chloride complexes occurred at ambient temperature and upon placing under an atmosphere of CO (1 atm), the desired rhodium(I) carbonyl derivatives were formed rapidly (t < 30 min) and isolated from solution in high yield (**3a**, 75 %; **4a**, 85 %). The formation of **3a** is associated with a downfield shift of the corresponding ^{31}P doublet resonance from δ = 46.6 to 63.9, alongside reduction of the $^1J_{RhP}$ coupling constant from 145 to 120 Hz (FB), whilst that of **4a** is marked visually by its characteristic dark green colour. Both complexes were comprehensively characterised using NMR and IR spectroscopy (vide infra), mass spectrometry, combustion analysis, and – in the case of **3a** – single-crystal X-ray diffraction (Figure 2). Unfortunately, despite our repeated attempts, we have so far been unable to grow single crystals of **4a** suitable for structure elucidation in the solid state. The preparation of **3a** as a $[BF_4]^-$ salt has previously been reported using an alternative synthetic route, and the relevant spectroscopic data are in close agreement.[23]

In the case of the rhodium(III) trichloride complexes, halide abstraction proceeded rapidly at ambient temperature to afford formally 16 VE $\{Rh(pincer)Cl_2\}^+$ species in solution (t < 30 min), however, subsequent coordination of CO was remarkably sluggish (1 atm). Complete conversion to **3b** was achieved only after heating at 50 °C for 5 days, whilst for **4b** vigorous stirring for 18 hours at ambient temperature was required. Both novel complexes were comprehensively characterised using NMR and IR spectroscopy (vide infra), mass spectrometry, combustion analysis, and single-crystal X-ray diffraction (Figure 2). The spectroscopic data of **3b** and **4b** are consistent with adoption of the expected C_{2v} (time averaged) and C_2 symmetric structures in solution, respectively, with formation of the former substantiated by ^{31}P NMR spectroscopy, with a doublet resonance at δ = 65.5 and $^1J_{RhP}$ coupling constant of 72 Hz (FB). The X-ray structures of **3b** and **4b** likewise corroborate octahedral structural formulations with *trans*-disposed chloride ligands in the solid state, with the most salient feature being disparate *Rh–CO* bond lengths of 1.884(3) and 1.931(10) Å, respectively. The former is notably elongated in comparison to its rhodium(I) analogue **3a** [1.828(3) Å].

Supplementing the aforementioned protocols, interconversion between the rhodium(I) and rhodium(III) carbonyl complexes was possible in THF at ambient temperature, through oxidation using $PhICl_2$ and reduction over activated zinc powder (Scheme 1). These redox reactions proceeded in quantitative spectroscopic yield.

2. Spectroscopic Handles

Spectroscopic data for the homologous series of Rh^I (**1a**–**4a**) and Rh^{III} (**1b**–**4b**) carbonyl complexes was acquired under equivalent conditions. For meaningful analysis of IR spectroscopic data this is particularly important as the medium is known to have a profound effect on the location of ν(CO) bands.[8,24,25] Dichloromethane solvent was chosen for reasons of operational simplicity, chemical compatibility, and in recognition of its common use in the acquisition of IR spectroscopic data for late transition metal complexes. The resulting data is compiled in Table 1 and discussed in turn below.

Comparison of the IR spectra reveals the expected trend for the Rh^I/Rh^{III} pairs, with the latter characterised by considerably higher ν(CO) values [Δν(CO) = 110–130 cm^{-1}]. The stretching frequencies of the Rh^I complexes show considerable variance and suggest increasing *net* donor strength in the order: (*R*,*R*)-Ph-pybox (2019 cm^{-1}) < *i*Pr-PNP (1998 cm^{-1}) < C–N–C–12

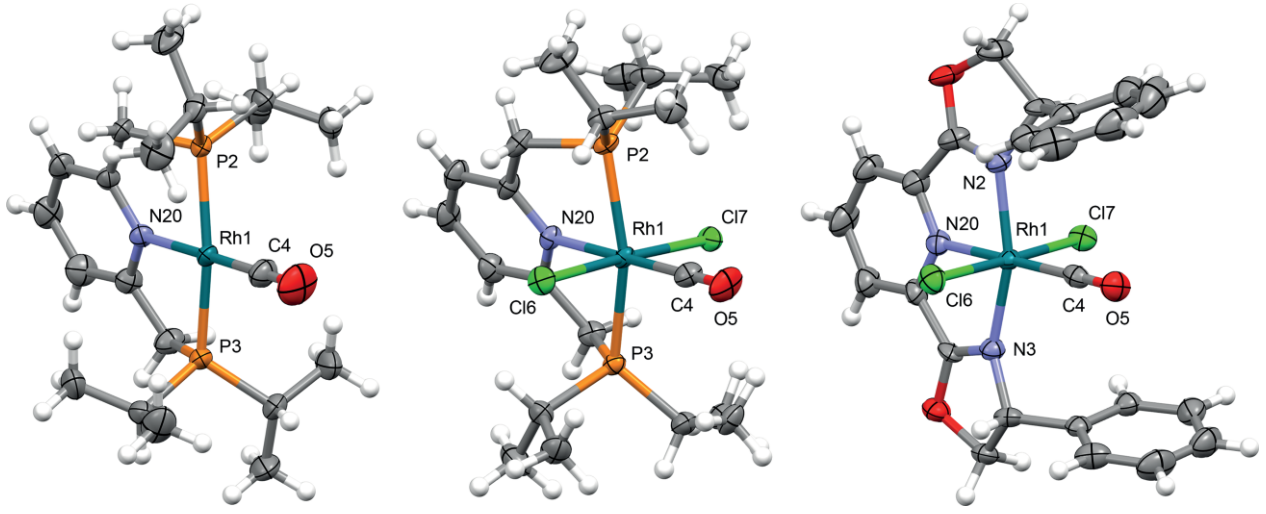

Figure 2. Solid-state structures of **3a** (left), **3b** (centre), and **4b** (right). Thermal ellipsoids drawn at 50 % probability; anion for all three structures omitted. Selected bond lengths (Å) and angles (°): **3a**, Rh1–P2, 2.2809(6); Rh1–P3, 2.2796(6); Rh1–C4, 1.828(3); Rh1–N20, 2.0923(19); P2–Rh1–P3, 165.84(2); N20–Rh1–C4, 178.38(11). **3b**, Rh1–P2, 2.3740(7); Rh1–P3, 2.3719(7); Rh1–C4, 1.884(3); Rh1–Cl6, 2.3397(7); Rh1–Cl7, 2.3523(7); Rh1–N20, 2.085(2); P2–Rh1–P3, 161.88(2); N20–Rh1–C4, 177.71(11); Cl6–Rh1–Cl7, 177.06(3). **4b**, Rh1–N2, 2.043(8); Rh1–N3, 2.016(8); Rh1–C4, 1.931(10); Rh1–Cl6, 2.326(3); Rh1–Cl7, 2.324(3); Rh1–N20, 1.990(8); N2–Rh1–N3, 157.7(3); N20–Rh1–C4, 179.0(5); Cl6–Rh1–Cl7, 177.85(11).

Table 1. Selected spectroscopic and structural parameters associated with complexes **1**–**4**.[a]

Complex	ν(CO) /cm^{-1}		δ_{13C}(CO)	$^1J_{RhC}$(CO)	*r*(CO) /Å		*r*(*Rh*CO) /Å		∠ DRhD /°		py tilt /°[c]	
	Expt.	DFT[b]		/Hz	Expt.	DFT	Expt.	DFT	Expt.	DFT	Expt.	DFT
1a	1979	2110	194.0	80	1.148(5)	1.142	1.804(3)	1.827	172.77(12)	171.82	38.58(10)	38.65
2a	1986	2116	196.8	78	1.154(5)	1.140	1.836(4)	1.852	155.18(15)	155.06	0.07(14)	0.00
3a	1998	2123	193.0	69	1.142(3)	1.139	1.828(3)	1.841	165.84(2)	165.85	13.68(7)	12.69
4a	2019	2158	188.1	77	–	1.134	–	1.878	–	154.93	–	0.99
1b	2110	2224	180.7	57	–	1.126	–	1.869	–	174.69	–	32.49
2b	2111	2220	181.6	57	[29]	1.126	[29]	1.900	156.47(12)	157.14	3.07(11)	0.00
3b	2110	2223	179.7	54	1.132(4)	1.125	1.884(3)	1.895	161.88(2)	163.53	21.81(7)	19.43
4b	2151	2268	171.8	55	1.117(13)	1.120	1.931(10)	1.940	157.7(3)	156.00	2.8(4)	1.72

[a] Calculated parameters for **1** and **2** use truncated pincer ligand models, **1′** and **2′**. IR data acquired in CH_2Cl_2 solution, NMR data acquired in CD_2Cl_2. [b] Unscaled values. [c] Angle between the least-squares mean planes of the py donor group and the RhD_2NC atoms.

(1986 cm^{-1}) < C^N^C–12 (1979 cm^{-1}) (Figure 1), in line with expectation based on the known ligand characteristics of the terminal donors. Although the corresponding Rh^{III} values are spread over a similar range, they do little to substantiate this trend: those of **1b**–**3b** are indistinguishable within nominal resolution limits, while **4b** is remarkably found at higher frequency than free CO (2151 vs. 2143 cm^{-1}). This "non-classical" behaviour, invoking very weak π-back bonding and C←O polarisation of the π bonding orbitals by the cationic metal fragment, is generally associated with complexes of the coinage metals and there are only a small number of rhodium precedents.[26–28] Consistent with the IR data, the crystallographically determined C–O bond length of **4b** is the only shortened compared to free CO [1.117(13) vs. 1.128 Å].

There are modest negative correlations of the ν(CO) values with the data acquired by ^{13}C NMR spectroscopy [δ_{13}(CO), R^2 = 0.95; $^1J_{RhC}$, R^2 = 0.89], but these are largely reflective of large differences observed between the Rh^{I} and Rh^{III} variants, rather than more interesting subtleties associated with variation of the pincer ligand; especially in the case of the $^1J_{RhC}$ values. Indeed, there is no appreciable correlation of the NMR parameters for the individual Rh^{I} and Rh^{III} data sets (R^2 < 0.25).

3. Computational analysis

To gain deeper insight into the relationship between the values of ν(CO) measured for **1**–**4** and the donor abilities of the corresponding pincer ligands we turned to DFT calculations, employing Grimme's dispersion corrected ωB97X-D3 functional and the extended transition state method for energy decomposition analysis combined with the natural orbitals for chemical valence theory (ETS-NOCV), as implemented in ORCA 4.1.0.[30–39] For computational simplicity, truncated models of the CNC pincer ligands were studied whereby the terminal NHC-donors are substituted with methyl groups, viz. C^N^C-Me (**1′**) and C-N-C-Me (**2′**). As vindication of this combined approach, there is a very strong positive correlation between the (unscaled) computed and experimental carbonyl stretching frequencies (R^2 = 0.99). With the rhodium(I) analogues showing the most diagnostic values, the subsequent discussion is primarily focused on delineating the molecular orbital contributions between the {Rh(pincer)}$^+$/CO and {Rh(CO)}$^+$/pincer fragments of **1a′**–**4a** using the ETS-NOCV method.

Decomposition of the metal-carbonyl interactions in **1a′**–**4a** enables delineation of both σ-donation and π-back bonding

contributions, which are found to be of approximately equal magnitude and together account for > 90 % of the interfragment orbital stabilisation energy (ΔE_{orb}, Table 2). In energetic terms, the strongest interactions are calculated in **1a′**, whilst the weakest are found in **4a**. Consideration of the total π-back bonding alone is not sufficient to reconcile the observed trends in carbonyl stretching frequency, with **2a′** and **3a** notably showing near identical sums. Instead significant contributions resulting from σ-bonding are implied, as these are considerably more pronounced in the PNP complex **3a** compared to CNC complex **2a′**. Similar trends are observed in the energy decomposition analysis of metal-carbonyl interactions of **1b′**–**4b**, although in line with expectation these are characterised by enhanced σ-donation (ΔE = +11 to +20 kcal mol^{-1}), significantly reduced π-back bonding (ΔE = −18 to −21 kcal mol^{-1}), and overall smaller ΔE_{orb} values (see supporting information). Greatest insight is instead obtained from decomposition of the metal-pincer interaction, where σ-donation accounts for the majority of the interfragment orbital stabilisation energy (> 60 %), but significant effects resulting from the conformation of the pincer backbone become apparent (Table 3). For instance, from this data the σ-donating capacity of the pincer types clearly increases in the order NNN < PNP < CNC, however, it is with the planar C-N-C rather than the more twisted C^N^C NHC-based variant

Table 2. Calculated orbital stabilisation energies for the {Rh(pincer)}$^+$/CO fragmentation of **1a′**–**4a** (kcal mol^{-1}).[a]

	σ({RhL}$^+$←CO)	π({RhL}$^+$→CO)$^\perp$	π({RhL}$^+$→CO)$^\parallel$	Σπ({RhL}$^+$→CO)	Total (ΔE_{orb})
1a′	−52.3	−27.6	−24.6	−52.2	−114.6
2a′	−47.2	−23.6	−24.8	−48.5	−103.6
3a	−52.1	−25.5	−23.5	−49.0	−108.8
4a	−46.0	−20.3	−19.9	−40.2	−93.3

[a] The characters of the interactions are classified from visual inspection of the NOCV orbitals; into carbonyl donation of local σ-symmetry and out-of-plane (⊥) and in-plane (||) π-back bonding.

Table 3. Calculated orbital stabilisation energies for the {Rh(CO)}$^+$/pincer fragmentation of **1a′**–**4a** (kcal mol^{-1}).[a]

	σ(L→ {Rh(CO)}$^+$)	π(L←{Rh(CO)}$^+$)^D	π(L←{Rh(CO)}$^+$)^{py}	Σπ(L←{Rh(CO)}$^+$)	Total (ΔE_{orb})
1a′	−176.0	−28.8	−7.6	−36.4	−240.1
2a′	−176.9	−29.9	−11.4	−41.3	−245.5
3a	−157.6	−43.6	−7.0	−50.6	−234.5
4a	−124.7	−31.3	−11.3	−42.6	−198.5

[a] The characters of the interactions are classified from visual inspection of the NOCV orbitals; into pincer ligand donation of local σ-symmetry and π-back bonding into the terminal (D) and central pyridyl (py) donor groups.

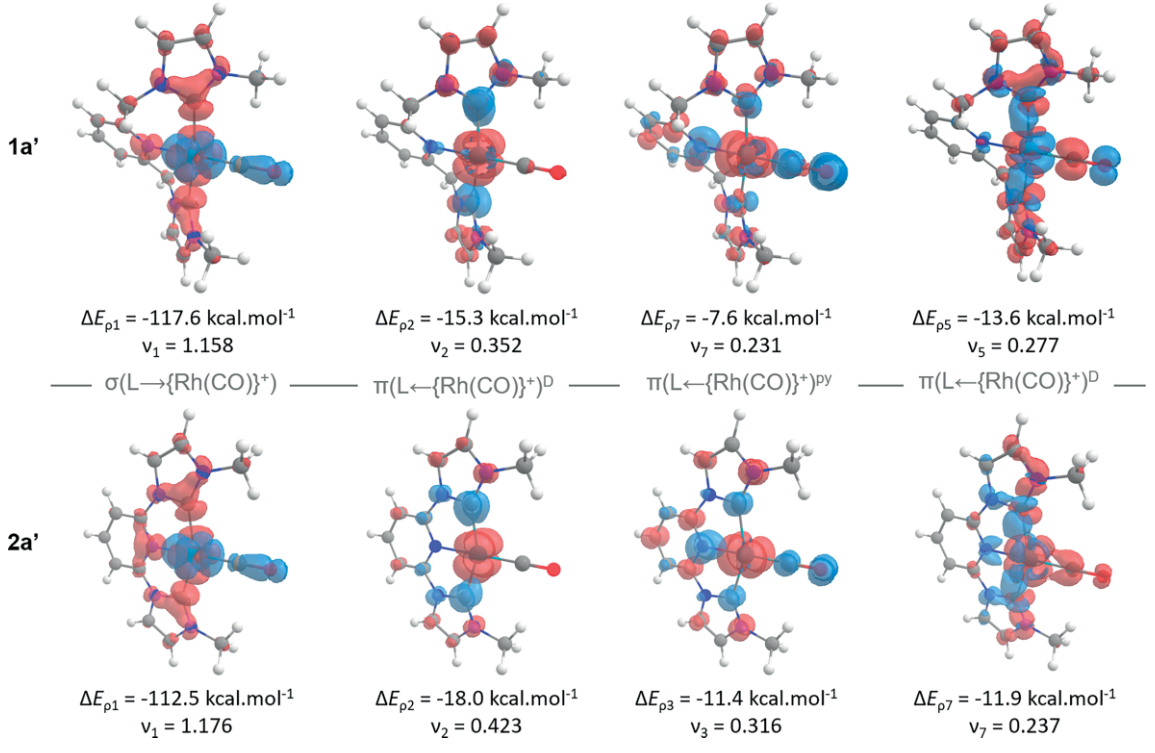

Figure 3. Selected deformation densities associated with the σ-donor and π-acidity of the CNC pincer ligands in **1a′** and **2a′**. Charge flow from red to blue.

that this type of bonding is the most pronounced (Figure 3). The degree of π-back bonding with the central pyridyl donor is also appreciably lower in **1a′** and **3a** and linked to twisting out of the coordination plane; a conformation adopted due to the presence of methylene spacers in the pincer backbone (Table 1, Figure 3). Of the bonding interactions, this divergence in π-acidity between the CNC-based pincer ligands is the most significant and we believe responsible for the observed order in *net* donor ability inferred spectroscopically for **1a**/**2a**.

The nuanced nature of the bonding contributions inferred from the ETS-NOCV analysis would therefore suggest that interpretation of the carbonyl stretching frequencies of the Rh^{I} carbonyl complexes is not straightforward in the context of tuning the reactivity of pincer complexes. For instance, the carbonyl stretching frequencies of **1a**–**4a** do not correlate with calculated thermodynamics of their oxidation to **1b**–**4b**, which are more exergonic in the order: PNP (–40.1 kcal mol^{-1}) < C-N-C (–45.6 kcal mol^{-1}) < NNN (–47.9 kcal mol^{-1}) < C^N^C (–50.1 kcal mol^{-1}). These values instead correlate much better with the corresponding differences in carbonyl stretching frequencies Δν(CO) (R^2 = 0.91), suggesting that this may be a more useful experimentally derived parameter.

Conclusions

To assemble a homologous series of pincer complexes of the form [Rh(pincer)(CO)][BAr^F_4] and [Rh(pincer)Cl_2(CO)][BAr^F_4], four new rhodium(I) and rhodium(III) carbonyl complexes of pyridyl-based pincer ligands with flanking phosphine (*i*Pr-PNP) and oxazoline [(*R*,*R*)-Ph-pybox] donors have been prepared. This was achieved by halide abstraction from the corresponding rhodium(I) chloride and rhodium(III) trichloride complexes followed by reaction with carbon monoxide, but interconversion between the Rh^{I}/Rh^{III} redox pairs can also be mediated through oxidation using $PhICl_2$ and reduction over activated zinc powder at RT. The new members were extensively characterised in solution, with the NMR (δ_{13C}, $^1J_{RhC}$) and IR [ν(CO)] spectroscopic properties associated with coordination of CO to rhodium critically analysed in comparison to those of established NHC-based pincer variants (twisted C^N^C-12 and planar C-N-C-12).

Whilst clear trends in the spectroscopic data can be drawn for Rh^{I}/Rh^{III} congeners, more interesting differences associated with variation of the pincer ligand can only be discerned from the carbonyl stretching bands of the rhodium(I) complexes. This IR data suggests *net* donor strength increases in the order (*R*,*R*)-Ph-pybox < *i*Pr-PNP < C-N-C-12 < C^N^C-12. To gain deeper insight, a DFT-based energy decomposition analysis was performed and identified important bonding differences associated with the conformation of the pincer backbone, which clouds straightforward interpretation of the experimental IR data. Most notably, twisting of central pyridyl donor out of the coordination plane appreciably reduces the π-acidity of the pincer ligand. A correlation between the difference in carbonyl stretching frequencies Δν(CO) and calculated thermodynamics of the Rh^{I}/Rh^{III} redox pairs was identified and could prove to be a useful mechanistic tool.

Experimental Section

1. General methods: All manipulations were performed under an atmosphere of argon using Schlenk and glove box techniques unless otherwise stated. Glassware was oven dried at 150 °C overnight and flame-dried under vacuum prior to use. Molecular sieves were activated by heating at 300 °C in vacuo overnight. Fluorobenzene (FB) was pre-dried with Al_2O_3, distilled from calcium hydride and dried twice over 3 Å molecular sieves. Tetrahydrofuran (THF) was distilled from sodium benzophenone then freeze-pump-thaw degassed and stored over 3 Å molecular sieves. CD_2Cl_2 was freeze-pump-thaw degassed and dried with 3 Å molecular sieves. Other anhydrous solvents were purchased from Acros Organics or Sigma-Aldrich, freeze-pump-thaw degassed and stored over 3 Å molecular sieves. Carbon monoxide was used from commercial supplier without further purification. Zn powder was activated from reaction with 1,2-dibromoethane in THF then dried and stored under argon. $[Rh(COE)_2Cl]_2$,[40] Na[BAr^F_4],[41] $PhICl_2$,[20] *i*Pr-PNP[42] and (*R*,*R*)-Ph-pybox[43] were synthesised according to published procedures. NMR spectra were recorded on Bruker spectrometers under argon at 298 K unless otherwise stated. Chemical shifts are quoted in ppm and coupling constants in Hz. NMR spectra in FB and THF were recorded using an internal capillary of C_6D_6.[19] IR spectra were recorded in CH_2Cl_2 using a KBr transmission cell and Jasco FT-IR-4700 spectrometer. ESI-MS were recorded on a Bruker MaXis mass spectrometer. Microanalyses were performed at the London Metropolitan University by Stephen Boyer.

2. Preparation of [Rh(*i*Pr-PNP)Cl]: *Adapted from a literature procedure.*[21] A solution of *i*Pr-PNP (215 mg, 0.63 mmol) and $[Rh(COE)_2Cl]_2$ (226 mg, 0.31 mmol) in toluene (30 mL) was stirred at ambient temperature for 3 h. The volatiles were removed in vacuo to leave a red oily residue which was redissolved in a minimal amount of toluene and layered with *n*-hexane to afford the product as red needles on diffusion, some of which were suitable for analysis using X-ray diffraction. Yield: 121 mg (40 %). The spectroscopic data is consistent with literature. ^{1}H NMR (300 MHz, C_6D_6): δ = 6.90 (t, $^3J_{HH}$ = 7.7, 1H, py), 6.30 (d, $^3J_{HH}$ = 7.7, 2H, py), 2.44 (vt, J_{PH} = 3.6, 4H, CH_2), 2.09 (appt sept, $^3J_{HH}$ = 7, 4H, CH), 1.52 (appt q, J = 8, 12H, CH_3), 1.07 (appt q, J = 7, 12H, CH_3). ^{31}P{^{1}H} NMR (121 MHz, C_6D_6): δ = 46.7 (d, $^1J_{RhP}$ = 145).

3. Preparation of [Rh((*R*,*R*)-Ph-pybox)Cl]: A solution of (*R*,*R*)-Ph-pybox (443 mg, 1.2 mmol) and $[Rh(COE)_2Cl]_2$ (431 mg, 0.6 mmol) in THF (50 mL) was stirred for 1 h. The suspension was left to settle for 48 h, before the solid was isolated by filtration and washed with cold THF (3 × 10 mL, –78 °C) to afford the product as a dark sparingly soluble blue-black solid. Yield: 526 mg (86 %). ^{1}H NMR (400 MHz, C_6D_6): δ = 7.64 (t, $^3J_{HH}$ = 7.8, 1H, py), 7.51 (d, $^3J_{HH}$ = 7.3, 4H, Ph), 7.10 (appt t, $^3J_{HH}$ = 8, 4H, Ph), 7.01 (t, $^3J_{HH}$ = 8, 2H, Ph), 6.85 (d, $^3J_{HH}$ = 7.8, 2H, py), 5.46 (dd, $^3J_{HH}$ = 9.6, 5.0, 2H, ox{CH}), 4.22 (dd, $^2J_{HH}$ = 8.8, $^3J_{HH}$ = 5.0, 2H, ox{CH_2}), 4.10 (appt t, J_{HH} = 9, 2H, ox{CH_2}). Acquisition of ^{13}C NMR data was encumbered by low solubility in C_6D_6. HR ESI-MS (MeOH, 180 °C, 3 kV) positive ion: 508.0293 ([*M* + H]$^+$, calcd. 508.0294) *m*/*z*. Anal. Calcd for $C_{23}H_{19}ClN_3O_2Rh$ (507.78 g mol^{-1}): C, 54.40; H, 3.77; N, 8.28; found C, 54.16; H, 4.07; N, 8.13.

4. Preparation of [Rh(*i*Pr-PNP)Cl_3]: A solution of [Rh(*i*Pr-PNP)Cl] (38 mg, 80 μmol) and $PhICl_2$ (23 mg, 83 μmol) in toluene (5 mL) was stirred at ambient temperature for 1 h. The resulting precipitate was isolated by filtration and dried to afford the product as an orange powder. Yield: 41 mg (84 %). Single crystals suitable for X-ray diffraction were obtained by slow diffusion of *n*-hexane into a solution of [Rh(*i*Pr-PNP)Cl_3] in dichloromethane (or THF) at ambient temperature. ^{1}H NMR (500 MHz, CD_2Cl_2): δ = 7.61 (t, $^3J_{HH}$ = 7.8, 1H,

py), 7.31 (d, $^3J_{HH}$ = 7.8, 2H, py), 3.92 (vt, J_{PH} = 4.3, 4H, CH_2), 3.17 (appt sept-vt, $^3J_{HH}$ = 7, J_{PH} = 4, 4H, CH), 1.51 (appt q, J = 8, 12H, CH_3), 1.47 (appt q, J = 7, 12H, CH_3). $^{13}C\{^1H\}$ NMR (126 MHz, CD_2Cl_2): δ = 164.4 (vt, J_{PC} = 4, py), 138.7 (s, py), 122.2 (vt, J_{PC} = 5, py), 39.2 (vt, J_{PC} = 10, CH_2), 25.0 (vt, J_{PC} = 11, CH), 19.7 (s, CH_3), 19.2 (s, CH_3). $^{31}P\{^1H\}$ NMR (121 MHz, CD_2Cl_2): δ = 41.0 (d, $^1J_{RhP}$ = 85). Anal. Calcd for $C_{19}H_{35}Cl_3NP_2Rh$ (548.70 g mol^{-1}): C, 41.59; H, 6.43; N, 2.55; found C, 41.60; H, 6.40; N, 2.51. HR ESI-MS (MeCN, 180 °C, 4 kV) positive ion: 570.0250 ([M + Na]$^+$, calcd. 570.0258) m/z.

5. Preparation of [Rh{(*R*,*R*)-Ph-pybox}Cl$_3$]: A solution of [Rh((*R*,*R*)-Ph-pybox)Cl] (50 mg, 98 µmol) and $PhICl_2$ (27 mg, 98 µmol) was stirred in CH_2Cl_2 (10 mL) for 18 h at ambient temperature. The product was precipitated with pentane (20 mL), isolated by filtration, and washed with pentane (3 × 10 mL) to afford the product as a dark orange solid. Yield: 45 mg (79 %). The spectroscopic data is consistent with literature.[22] ^1H NMR (500 MHz, CD_2Cl_2): δ = 8.36 (t, $^3J_{HH}$ = 8.0, 1H, py), 8.17 (d, $^3J_{HH}$ = 8.1, 2H, py), 7.53–7.45 (m, 4H, Ph), 7.38–7.32 (m, 6H, Ph), 5.54 (appt t, $^3J_{HH}$ = 11, 2H, ox{CH}), 5.42 (appt t, J_{HH} = 11, 2H, ox{CH_2}), 4.92 (appt t, J_{HH} = 9, 2H, ox{CH_2}).

6. NMR scale reactions: synthesis of carbonyl complexes: A suspension of [LRhCl_n] (10 mM) (L = *i*Pr-PNP, (*R*,*R*)-Ph-pybox; n = 1, 3) and Na[BAr$^F{}_4$] (10 mM) in FB inside a J. Young's valve NMR tube was mixed at ambient temperature and periodically monitored by NMR spectroscopy. Once halide abstraction was complete, the solution was freeze-pump-thaw degassed, placed under an atmosphere of CO, and mixed until complete conversion to the rhodium carbonyl product was confirmed by NMR spectroscopy. The associated reaction timeframes were used to inform the preparation procedures that are outlined below.

7. Preparation of [Rh(*i*Pr-PNP)(CO)][BAr$^F{}_4$] (3a): A suspension of [Rh(*i*Pr-PNP)Cl] (10 mg, 21 µmol) and Na[BAr$^F{}_4$] (20 mg, 23 µmol) in FB (1 mL) was stirred at ambient temperature for 24 h. The resulting pale yellow solution was filtered, freeze-pump-thaw degassed, placed under an atmosphere of CO, and held at ambient temperature for 30 min. The volatiles were removed in vacuo to give an oily residue which was dissolved in a minimal amount of dichloromethane and layered with *n*-hexane to afford the product as yellow crystals on diffusion, some of which were suitable for X-ray diffraction. Yield: 22 mg (75 %). ^1H NMR (500 MHz, CD_2Cl_2): δ = 7.80 (t, $^3J_{HH}$ = 7.8, 1H, py), 7.74–7.69 (m, 8H, Ar^F), 7.57–7.53 (br, 4H, Ar^F), 7.46 (d, $^3J_{HH}$ = 7.8, 2H, py), 3.66 (vt, J_{PH} = 4, 4H, CH_2), 2.37 (appt sept-vt, $^3J_{HH}$ = 6, J_{PH} = 3, 4H, CH), 1.30 (appt q, J = 7, 12H, CH_3), 1.18 (appt q, J = 7, 12H, CH_3). ^1H NMR (300 MHz, C_6H_5F, selected data): δ = 3.13 (vt, J_{PH} = 3, 4H, CH_2), 1.95–1.81 (m, 4H, CH), 1.00 (appt q, J = 8, 12H, CH_3), 0.85 (appt q, J = 7, 12H, CH_3). $^{13}C\{^1H\}$ NMR (126 MHz, CD_2Cl_2): δ = 193.0 (dt, $^1J_{RhC}$ = 69 and $^2J_{PC}$ = 14, RhCO), 164.5 (vt, J_{PC} = 6, py) 162.1 (q, $^1J_{CB}$ = 50, Ar^F), 141.0 (s, py), 135.2 (s, Ar^F), 129.3 (qq, $^2J_{FC}$ = 32 and $^3J_{CB}$ = 3, Ar^F), 125.0 (q, $^1J_{FC}$ = 272, CF_3) 122.3 (vt, J_{PC} = 6, py), 117.9 (sept, $^3J_{FC}$ = 4, Ar^F), 35.9 (vt, J_{PC} = 10, CH_2), 25.7 (vtd, J_{PC} = 13 and $^2J_{RhC}$ = 2, CH), 19.4 (vt, J_{PC} = 3, CH_3), 18.4 (s, CH_3). $^{31}P\{^1H\}$ NMR (121 MHz, CD_2Cl_2): δ = 64.4 (d, $^1J_{RhP}$ = 120). $^{31}P\{^1H\}$ NMR (121 MHz, C_6H_5F): δ = 63.9 (d, $^1J_{RhP}$ = 120). Anal. Calcd for $C_{52}H_{47}BF_{24}NOP_2Rh$ (1333.58 g mol^{-1}): C, 46.83; H, 3.55; N, 1.05; found C, 46.70; H, 3.47; N, 0.97. HR ESI-MS (MeCN, 180 °C, 4 kV) positive ion: 470.1246 ([M]$^+$, calcd. 470.1243) m/z. FT-IR (CH_2Cl_2): ν(CO) 1998 cm^{-1}.

8. Preparation of [Rh(*i*Pr-PNP)Cl$_2$(CO)][BAr$^F{}_4$] (3b): A suspension of [Rh(*i*Pr-PNP)Cl_3] (20 mg, 37 µmol) and Na[BAr$^F{}_4$] (35 mg, 39 µmol) in FB (1 mL) was stirred at ambient temperature for 1 h. The resulting pale yellow solution was filtered, freeze-pump-thaw degassed, placed under an atmosphere of CO, and stirred at 50 °C for 5 days. The volatiles were removed in vacuo to give an oily residue which was dissolved in minimal amount of dichloromethane and layered with *n*-hexane to afford the product as light yellow crystals on diffusion, some of which were suitable for X-ray diffraction. Yield: 41 mg (79 %). ^1H NMR (500 MHz, CD_2Cl_2): δ = 7.94 (t, $^3J_{HH}$ = 7.8, 1H, py), 7.74–7.70 (m, 8H, Ar^F), 7.58–7.56 (obscured, 2H, py), 7.56 (br, 4H, Ar^F), 4.14 (vt, J_{PH} = 4.7, 4H, CH_2), 3.02 (appt sept-vt, $^3J_{HH}$ = 7, J_{PH} = 4, 4H, CH), 1.50 (appt q, J = 8, 12H, CH_3), 1.46 (appt q, J = 7, 12H, CH_3). ^1H NMR (300 MHz, C_6H_5F, selected data): δ = 3.65 (vt, J_{PH} = 5, 4H, CH_2), 2.72–2.56 (br, 4H, CH), 1.13 (appt q, J = 8, 24H, CH_3). $^{13}C\{^1H\}$ NMR (151 MHz, CD_2Cl_2): δ = 179.7 (d, $^1J_{RhC}$ = 54, RhCO; $^2J_{PC}$ coupling was not sufficiently resolved), 162.2 (q, $^1J_{CB}$ = 50, Ar^F), 161.9 (obscured, py), 142.2 (s, py), 135.2 (s, Ar^F), 129.3 (qq, $^2J_{FC}$ = 32 and $^3J_{CB}$ = 3, Ar^F), 125.0 (q, $^1J_{FC}$ = 272, CF_3) 124.0 (vt, J_{PC} = 5, py), 117.9 (sept, $^3J_{FC}$ = 4, Ar^F), 39.2 (vt, J_{PC} = 13, CH_2), 25.8 (vt, J_{PC} = 12, CH), 19.8 (s, CH_3), 19.0 (s, CH_3). $^{31}P\{^1H\}$ NMR (121 MHz, CD_2Cl_2): δ = 65.7 (d, $^1J_{RhP}$ = 72). $^{31}P\{^1H\}$ NMR (121 MHz, C_6H_5F): δ = 65.5 (d, $^1J_{RhP}$ = 72). Anal. Calcd for $C_{52}H_{47}BF_{24}Cl_2NOP_2Rh$ (1404.48 g mol^{-1}): C, 44.47; H, 3.37; N, 1.00; found C, 44.34; H, 3.25; N, 0.92. HR ESI-MS (MeCN, 180 °C, 4 kV) positive ion: 540.0619 ([M]$^+$, calcd. 540.0620) m/z. FT-IR (CH_2Cl_2): ν(CO) 2110 cm^{-1}.

9. Preparation of [Rh{(*R*,*R*)-Ph-pybox}(CO)][BAr$^F{}_4$] (4a): A suspension of [Rh((*R*,*R*)-Ph-pybox)Cl] (34 mg, 67 µmol) and Na[BAr$^F{}_4$] (63 mg, 70 µmol) in FB (10 mL) was prepared and immediately freeze-pump-thaw degassed, placed under an atmosphere of CO, and then stirred at ambient temperature for 30 min. The volatiles were removed in vacuo to give an oily residue, from which the product was extracted using dichloromethane (10 mL). The product was obtained as a foamy dark green solid on removal of the solvent, azeotroping with diethyl ether. Yield: 64 mg (85 %). ^1H NMR (500 MHz, CD_2Cl_2): δ = 8.19 (t, $^3J_{HH}$ = 8.0, 1H, py), 7.92 (d, $^3J_{HH}$ = 8.0, 2H, py), 7.78–7.66 (m, 8H, Ar^F), 7.56 (br, 4H, Ar^F), 7.48–7.35 (m, 6H, Ph), 7.27–7.21 (m, 4H, Ph), 5.32 (appt t, J_{HH} = 10, 2H, ox{CH_2}), 5.12 (appt t, $^3J_{HH}$ = 10, 2H, ox{CH}), 4.86 (appt t, J_{HH} = 9, 2H, ox{CH_2}). ^1H NMR (300 MHz, C_6H_5F, selected data): δ = 5.00 (appt t, J_{HH} = 9, 2H, ox{CH_2}), 4.77 (appt t, $^3J_{HH}$ = 10, 2H, ox{CH}), 4.49 (appt t, J_{HH} = 9, 2H, ox{CH_2}). $^{13}C\{^1H\}$ NMR (126 MHz, CD_2Cl_2): δ = 188.1 (d, $^1J_{RhC}$ = 77, RhCO), 167.5 (s, ox{OCN}), 162.1 (q, $^1J_{CB}$ = 50, Ar^F), 146.5 (s, py), 143.3 (s, py), 136.8 (s, Ph), 135.2 (s, Ar^F), 130.2 (s, Ph), 129.8 (s, Ph), 129.2 (qq, $^2J_{FC}$ = 32, $^3J_{CB}$ = 3, Ar^F), 128.0 (s, Ph), 125.5 (s, py), 125.0 (q, $^1J_{FC}$ = 272, Ar^F), 117.8 (sept, $^3J_{FC}$ = 4, Ar^F), 80.1 (s, ox{CH_2}), 69.8 (s, ox{CH}). HR ESI-MS (MeOH, 180 °C, 3 kV) positive ion: 500.0518 ([M]$^+$, calcd. 500.0521) m/z. Anal. Calcd for $C_{56}H_{31}BF_{24}N_3O_3Rh$ (1363.56 g mol^{-1}): C, 49.33; H, 2.29; N, 3.08; found C, 49.17; H, 2.38; N, 3.03. FT-IR (CH_2Cl_2): ν(CO) 2019 cm^{-1}.

10. Preparation of [Rh{(*R*,*R*)-Ph-pybox}Cl$_2$(CO)][BAr$^F{}_4$] (4b): A suspension of [Rh{(*R*,*R*)-Ph-pybox}Cl_3] (21 mg, 36 µmol) and Na[BAr$^F{}_4$] (34 mg, 38 µmol) in FB (10 mL) was prepared and immediately freeze-pump-thaw degassed, placed under an atmosphere of CO, and then stirred vigorously at ambient temperature for 18 h. The volatiles were removed in vacuo to give an oily residue, from which the crude product was extracted using dichloromethane (10 mL). The resulting solution was concentrated in vacuo and excess pentane added to precipitate the product, which was isolated by filtration, washed with pentane (3 × 10 mL) and dried. Yield: 37 mg (72 %, foamy lime green solid). Crystals suitable for X-ray diffraction were obtained by recrystallisation from dichloromethane/pentane. ^1H NMR (500 MHz, CD_2Cl_2) δ = 8.67 (t, $^3J_{HH}$ = 8.1, 1H, py), 8.40 (d, $^3J_{HH}$ = 8.1, 2H, py), 7.76–7.70 (m, 8H, Ar^F), 7.56 (br, 4H, Ar^F), 7.54–7.38 (m, 10H, Ph), 5.58 (appt t, J_{HH} = 10, 2H, ox{CH_2}), 5.43 (appt t, $^3J_{HH}$ = 12, 2H, ox{CH}), 5.04 (dd, $^2J_{HH}$ = 12.0, $^3J_{HH}$ = 9.4, 2H, ox{CH_2}). ^1H NMR (300 MHz, C_6H_5F, selected data): δ = 4.99 (appt t, J_{HH} = 11, 2H, ox{CH_2}), 4.75 (appt t, $^3J_{HH}$ = 10, 2H, ox{CH}), 4.37 (dd, $^2J_{HH}$ = 12.2, $^3J_{HH}$ = 9.5, 2H, ox{CH_2}). $^{13}C\{^1H\}$ NMR

(126 MHz, CD_2Cl_2): δ = 171.8 (d, $^1J_{RhC}$ = 55, RhCO), 168.2 (s, ox{OCN}), 162.2 (q, $^1J_{CB}$ = 50, Ar^F), 145.3 (s, py), 145.1 (s, py), 135.2 (s, Ar^F), 132.9 (s, Ph), 131.3 (s, Ph), 130.0 (s, Ph), 129.8 (s, py), 129.6 (s, Ph), 129.3 (qq, $^2J_{FC}$ = 32, $^3J_{CB}$ = 3, Ar^F), 125.0 (q, $^1J_{FC}$ = 272, Ar^F), 117.9 (sept, $^3J_{FC}$ = 4, Ar^F), 80.6 (s, ox{CH_2}), 69.4 (s, ox{CH}). HR ESI-MS (MeOH, 180 °C, 3 kV) positive ion: 623.9939 ([*M* + NaOMe]$^+$, calcd. 623.9935) *m/z*. Anal. Calcd for $C_{56}H_{31}BCl_2F_{24}N_3O_3Rh$ (1434.46 g mol^{-1}): C, 46.89; H, 2.18; N, 2.93; found C, 47.11; H, 2.10; N, 2.86. FT-IR (CH_2Cl_2): ν(CO) 2151 cm^{-1}.

11. NMR scale reactions: oxidative addition of Rh^I carbonyl complexes

11.1. [Rh(*i*Pr-PNP)(CO)][BAr^F_4] (3a): A solution of **3a** (6.7 mg, 5.0 µmol) and $PhICl_2$ (1.4 mg, 5.0 µmol) in THF (0.5 mL) within a J. Young's valve NMR tube was left at ambient temperature for 1 h to afford [Rh(*i*Pr-PNP)(CO)Cl_2][BAr^F_4] **3b** in quantitative spectroscopic yield. ^{1}H NMR (300 MHz, THF, selected data): δ = 8.41 (t, $^3J_{HH}$ = 7.7, 1H, py), 8.05 (d, $^3J_{HH}$ = 8.9, 2H, py) ^{31}P{^{1}H} NMR (121 MHz, THF): δ = 66.3 (d, $^1J_{RhP}$ = 71).

11.2. [Rh{(*R*,*R*)-Ph-pybox}(CO)][BAr^F_4] (4a): A solution of **4a** (6.9 mg, 5.0 µmol) and $PhICl_2$ (1.4 mg, 5.0 µmol) in THF (0.5 mL) within a J. Young's valve NMR tube was left at ambient temperature for 1 h to afford [Rh{(*R*,*R*)-Ph-pybox}(CO)Cl_2][BAr^F_4] **4b** in quantitative spectroscopic yield. ^{1}H NMR (300 MHz, THF, selected data): δ = 9.17 (t, $^3J_{HH}$ = 8.2, 1H, py), 9.01 (d, $^3J_{HH}$ = 8.1, 2H, py), 7.85–7.70 (m, 10H, Ph), 5.99 (appt t, J_{HH} = 10, 2H, ox{CH_2}), 5.82 (appt t, $^3J_{HH}$ = 11, 2H, ox{CH}), 5.41 (dd, $^2J_{HH}$ = 11.4, $^3J_{HH}$ = 9.1, 2H, ox{CH_2}).

12. NMR scale reactions: reduction of Rh^{III} carbonyl complexes

12.1. [Rh(*i*Pr-PNP)Cl_2(CO)][BAr^F_4] (3b): A suspension of **3b** (7.1 mg, 5.1 µmol) and Zn powder (0.7 mg, 10.1 µmol) in THF (0.5 mL) within a J. Young's valve NMR tube was left mixing at ambient temperature for 6 h to afford [Rh(*i*Pr-PNP)Cl(CO)][BAr^F_4] **3a** in quantitative spectroscopic yield. ^{1}H NMR (300 MHz, THF, selected data): δ = 8.27 (t, $^3J_{HH}$ = 7.9, 1H, py), 7.96–7.89 (obscured, 2H, py). ^{31}P{^{1}H} NMR (121 MHz, THF): δ = 64.9 (d, $^1J_{RhP}$ = 120).

12.2. [Rh{(*R*,*R*)-Ph-pybox}Cl_2(CO)][BAr^F_4] (4b): A suspension of **4b** (7.2 mg, 5.0 µmol) and Zn powder (0.6 mg, 10.7 µmol) in THF (0.5 mL) within a J. Young's valve NMR tube was left mixing at ambient temperature for 1 h to afford [Rh{(*R*,*R*)-Ph-pybox}(CO)]-[BAr^F_4] **4a** in quantitative spectroscopic yield. ^{1}H NMR (300 MHz, THF, selected data): δ = 8.71 (t, $^3J_{HH}$ = 7.9, 1H, py), 8.47 (d, $^3J_{HH}$ = 7.9, 2H, py), 7.76–7.60 (m, 10H, Ph), 5.73 (appt t, J_{HH} = 10, 2H, ox{CH_2}), 5.55 (appt t, $^3J_{HH}$ = 10, 2H, ox{CH}), 5.22 (appt t, J_{HH} = 9, 2H, ox{CH_2}).

13. Crystallography

CCDC 1922373 {[Rh(*i*Pr-PNP)Cl]}, 1922374 {[Rh((*R*,*R*)-Ph-pybox)Cl]}, 1922375 {[Rh(*i*Pr-PNP)Cl_3].THF}, 1922376 {[Rh(*i*Pr-PNP)Cl_3].CH_2Cl_2}, 1922377 {[Rh((*R*,*R*)-Ph-pybox)Cl_3]}, 1922378 (**3a**), 1922379 (**3b**), and 1922380 (**4b**) contain the supplementary crystallographic data for this paper. These data can be obtained free of charge from The Cambridge Crystallographic Data Centre.

An analysis of the ligand steric effects, using a method developed by Guzei,[44] is provided in the Supporting Information.

14. Computational methods

Density functional theory calculations were carried out using the ORCA 4.1.0 program,[30,33] employing Grimme's dispersion corrected ωB97X-D3 functional[31,32] and the def2-TZVP(-f) basis set on all atoms, with the associated def2-ECP effective core potential on Rh.[34,35] The RIJCOSX approximation was used to reduce the computational cost of calculations (with the def2/J auxiliary basis set).[36,37] Geometries of metal cations were optimised starting from the X-ray data. Characterisation of stationary points as minima was verified by analytical vibrational mode analysis. Thermal corrections (298.15 K, 1 atm) were applied to deduce the Gibbs free energies. Coordination of the CO and pincer ligands was investigated using the extended transition state method for energy decomposition analysis combined with the natural orbitals for chemical valence theory (ETS-NOCV) as implemented in ORCA 4.1.0.[38,39]

Conflicts of interest

There are no conflicts to declare.

Supporting Information (see footnote on the first page of this article): NMR, IR and ESI-MS spectra of new compounds and selected reactions; further computational details and data; solid-state structures of [Rh(*i*Pr-PNP)Cl], [Rh((*R*,*R*)-Ph-pybox)Cl], [Rh(*i*Pr-PNP)Cl_3] and [Rh{(*R*,*R*)-Ph-pybox}Cl_3] (PDF). Optimized geometries (XYZ). Primary NMR data (MNOVA).

Acknowledgments

We thank the European Research Council (ERC, grant agreement 637313) and Royal Society (UF100592, UF150675, A. B. C.) for financial support. High-resolution mass-spectrometry data were collected using instruments purchased through support from Advantage West Midlands and the European Regional Development Fund. Crystallographic data were collected using an instrument that received funding from the ERC under the European Union's Horizon 2020 research and innovation programme (grant agreement No 637313). Computing facilities were provided by the Scientific Computing Research Technology Platform of the University of Warwick.

Keywords: Pincer ligands · Donor strength · Rhodium · Carbonyl ligands · Structure-property relationships

[1] D. Morales-Morales, *Pincer Compounds*, Elsevier, Amsterdam, **2018**.
[2] R. E. Andrew, L. González-Sebastián, A. B. Chaplin, *Dalton Trans.* **2016**, *45*, 1299–1305.
[3] M. E. Van Der Boom, D. Milstein, *Chem. Rev.* **2003**, *103*, 1759–1792.
[4] D. Benito-Garagorri, K. Kirchner, *Acc. Chem. Res.* **2008**, *41*, 201–213.
[5] A. Kumar, T. M. Bhatti, A. S. Goldman, *Chem. Rev.* **2017**, *117*, 12357–12384.
[6] E. Peris, R. H. Crabtree, *Chem. Soc. Rev.* **2018**, *47*, 1959–1968.
[7] C. A. Tolman, *J. Am. Chem. Soc.* **1970**, *92*, 2953–2956.
[8] C. A. Tolman, *Chem. Rev.* **1977**, *77*, 313–348.
[9] A. R. Chianese, X. Li, M. C. Janzen, J. W. Faller, R. H. Crabtree, *Organometallics* **2003**, *22*, 1663–1667.
[10] R. A. Kelly, H. Clavier, S. Giudice, N. M. Scott, E. D. Stevens, J. Bordner, I. Samardjiev, C. D. Hoff, L. Cavallo, S. P. Nolan, *Organometallics* **2008**, *27*, 202–210.
[11] S. Leuthäußer, D. Schwarz, H. Plenio, *Chem. Eur. J.* **2007**, *13*, 7195–7203.
[12] T. Dröge, F. Glorius, *Angew. Chem. Int. Ed.* **2010**, *49*, 6940–6952; *Angew. Chem.* **2010**, *122*, 7094.
[13] S. Wolf, H. Plenio, *J. Organomet. Chem.* **2009**, *694*, 1487–1492.
[14] A. Reinholdt, J. Bendix, *Inorg. Chem.* **2017**, *56*, 12492–12497.
[15] H. V. Huynh, Y. Han, R. Jothibasu, J. A. Yang, *Organometallics* **2009**, *28*, 5395–5404.
[16] L. Maser, C. Schneider, L. Vondung, L. Alig, R. Langer, *J. Am. Chem. Soc.* **2019**, *141*, 7596–7604.
[17] J. J. Davidson, J. C. Demott, C. Douvris, C. M. Fafard, N. Bhuvanesh, C. H. Chen, D. E. Herbert, C. I. Lee, B. J. McCulloch, B. M. Foxman, O. V. Ozerov, *Inorg. Chem.* **2015**, *54*, 2916–2935.
[18] R. E. Andrew, A. B. Chaplin, *Inorg. Chem.* **2015**, *54*, 312–322.

[19] S. D. Pike, M. R. Crimmin, A. B. Chaplin, *Chem. Commun.* **2017**, *53*, 3615–3633.
[20] J. Yu, C. Zhang, *Synthesis* **2009**, *2009*, 2324–2328.
[21] M. Feller, Y. Diskin-Posner, G. Leitus, L. J. W. Shimon, D. Milstein, *J. Am. Chem. Soc.* **2013**, *135*, 11040–11047.
[22] H. Nishiyama, M. Kondo, T. Nakamura, K. Itoh, *Organometallics* **1991**, *10*, 500–508.
[23] M. Feller, Y. Diskin-Posner, L. J. W. Shimon, E. Ben-Ari, D. Milstein, *Organometallics* **2012**, *31*, 4083–4101.
[24] D. G. Gusev, *Organometallics* **2009**, *28*, 763–770.
[25] O. Kühl, *Coord. Chem. Rev.* **2005**, *249*, 693–704.
[26] A. J. Lupinetti, S. H. Strauss, G. Frenking, *Prog. Inorg. Chem.* **2001**, *49*, 1–112.
[27] G. Frenking, C. Loschen, A. Krapp, F. A. U. Stefan, S. H. Strauss, *J. Comput. Chem.* **2007**, *28*, 117–126.
[28] G. Bistoni, S. Rampino, N. Scafuri, G. Ciancaleoni, D. Zuccaccia, L. Belpassi, F. Tarantelli, *Chem. Sci.* **2016**, *7*, 1174–1184.
[29] These metrics are not chemically sensible and appear to be effected by crystallographic artefacts.
[30] F. Neese, *Wiley Interdiscip. Rev.: Comput. Mol. Sci.* **2012**, *2*, 73–78.
[31] S. Grimme, J. Antony, S. Ehrlich, H. Krieg, *J. Chem. Phys.* **2010**, *132*, 263–272.
[32] Y.-S. Lin, G.-D. Li, S.-P. Mao, J.-D. Chai, *J. Chem. Theory Comput.* **2013**, *9*, 263–272.
[33] F. Neese, *Wiley Interdiscip. Rev.: Comput. Mol. Sci.* **2018**, *8*, e1327.
[34] F. Weigend, R. Ahlrichs, *Phys. Chem. Chem. Phys.* **2005**, *7*, 3297–3305.
[35] T. Leininger, A. Nicklass, W. Küchle, H. Stoll, M. Dolg, A. Bergner, *Chem. Phys. Lett.* **1996**, *255*, 274–280.
[36] F. Neese, F. Wennmohs, A. Hansen, U. Becker, *Chem. Phys.* **2009**, *356*, 98–109.
[37] F. Weigend, *Phys. Chem. Chem. Phys.* **2006**, *8*, 1057–1065.
[38] M. P. Mitoraj, A. Michalak, T. Ziegler, *J. Chem. Theory Comput.* **2009**, *5*, 962–975.
[39] A. Altun, F. Neese, G. Bistoni, *J. Chem. Theory Comput.* **2019**, *15*, 215–228.
[40] A. van der Ent, A. L. Onderdelinden, R. A. Schunn, in *Inorg. Synth.*, John Wiley & Sons, Ltd, **1990**, pp. 90–92.
[41] W. E. Buschman, J. S. Miller, K. Bowman-James, C. N. Miller, in *Inorg. Synth.*, John Wiley & Sons, Ltd, **2002**, pp. 75–121.
[42] W. P. Leung, Q. W. Y. Ip, S. Y. Wong, T. C. W. Mak, *Organometallics* **2003**, *22*, 4604–4609.
[43] J. Guo, B. Wang, J. Bi, C. Zhang, H. Zhang, C. Bai, Y. Hu, X. Zhang, *Polymer* **2015**, *59*, 124–132.
[44] I. A. Guzei, M. Wendt, *Dalton Trans.* **2006**, 3991–3999.

Received: July 5, 2019